Effect of the doping concentration on the zero-field spin splitting and Rashba parameter in a *p*-InAs MOSFET

Saadi Lamari*
Département de Physique, Faculté des Sciences, Université Ferhat Abbas, Sétif 19000DZ, Algeria
(Manuscript received on 9 May 2002; revised manuscript received 25 July 2002; published 30 April 2003)

Using the Hartree approximation, the 8×8 Kane Hamiltonian, and the envelope-function scheme the electronic structure of electrons bound within an inversion layer on *p*-InAs in a Mosfet geometry is computed self-consistently and studied as a function of the two-dimensional electron density N_S and the doping concentration N_A-N_D. The subband spin splitting δ_k^ν at an in-plane wave vector k varies almost linearly with N_S, and for the same electron density and k it is larger in the lower subbands. Likewise, the k-dependent subband Rashba parameter α_k^ν at a given k shows an analogous behavior. Varying the doping concentration in the interval 1.8×10^{15}–1.8×10^{17} cm^{-3}, in subband ν the spin-splitting δ_ν at the Fermi level is computed for N_S in the range 10^{11}–4.8×10^{12} cm^{-2}, where it is found to be an increasing function of N_S; moreover, it is largest in the ground subband. At the Fermi level, the corresponding Rashba parameter α_ν is also computed as a function of N_S in both the ground and first excited subbands while N_A-N_D is varied from 0.433×10^{17} to 1.8×10^{17} cm^{-3}. In this range, whereas α_1 simply shows a decreasing trend as a function of N_S, α_0 exhibits new and counterintuitive N_S dependencies as N_A-N_D is varied. Moreover, α_1 can either be larger or smaller than α_0, even when tunneling into the barrier is completely neglected. In addition, the role of the first excited subband on the overall N_S dependence of α_0 turns out to be crucial.

DOI: 10.1103/PhysRevB.67.165329 PACS number(s): 73.40.Qv, 71.70.Ej, 73.61.Ey, 73.21.−b

I. INTRODUCTION

Following the seminal proposal of the spin-polarized transistor by Datta and Das[1] over ten years ago, the spin properties of semiconductor heterostructures have in recent years become the subject of intense theoretical[2–6] as well as experimental[7–17] investigations. In this newly suggested device, spin modulation of the source-drain (SD) current relies crucially on a spin-orbit coupling constant α, known as the Rashba parameter.[18] Furthermore, successful operation of this field-effect transistor (FET) is tributary to the extent to which this coefficient is tunable by the gate voltage[1] V_g.

Now, while it has customarily been thought that α is simply proportional[3,11,19] to the average electric-field strength $\langle\mathbf{E}\rangle$ felt by an electron within the quasi-two-dimensional (2D) electron gas, careful magnetoresistance measurements by different groups on different materials and systems cannot be reconciled with this simple picture.[9–12] For instance, Shubnikov–de Haas (SdH) measurements by Heida *et al.*[11] on an InAs/AlSb asymmetric gated quantum well led to a constant Rashba parameter regardless of V_g, which means that no tuning occurs. This surprising result remained unexplained, and the authors of this work simply speculated on the origin of the constancy. In addition, previous work by Nitta *et al.*[9] on an InGaAs/InAlAs heterostructure led to a decreasing behavior for α as V_g was increased, in agreement with the experimental results of Schäpers *et al.*[10] on an InGaAs/InP asymmetric gated quantum well. Furthermore, close analysis of the more recent data of Hu *et al.*[12] on an InGaAs/InAlAs gated asymmetric quantum well reveals that α in the ground subband actually decreases for low 2D electron density N_S then becomes roughly constant starting very nearly at densities around which the first excited subband populates. This work[12] explicitly recognizes the importance of nonparabolicity, and gives evidence for α in the first excited subband which is actually found to be larger than its counterpart in the ground subband, and while the latter is nearly constant the former instead decreases as N_S is increased. In this regard, it should, however, be emphasized that no explanations for these behaviors were given; moreover, on intituitive grounds one expects weaker average electric fields in higher subbands. Hence, were α simply proportional to the electric field, a smaller value in the first excited subband would have been obtained as compared to the ground subband and an increasing trend with N_S would have been expected.

In contrast to the above, using an InGaAs/InAlAs heterostructure with a different stoichiometry than that of Ref. 9, more recently Sato *et al.*[17] in fact found an increasing trend for α. Furthermore, work by Matsuyama *et al.*[13] on a *p*-InAs metal-oxide semiconductor field-effect transistor (MOSFET) also concluded that the Rashba parameter should be an increasing function of V_g, although in Ref. 5 different conclusions are drawn as regards this experiment.

In the interpretation of all the experimental work cited above, the authors seem, however, to underestimate the importance of subband population. In this regard, one should stress that as V_g varies, or equivalently as N_S changes,[20] both the average electric field as well as the Fermi level, and hence the corresponding Fermi wave vectors, at which α is indeed measured by transport experiments, also change. As a matter of fact, in a recent theoretical work by the present author[5] on the inversion layer on *p*-InAs in a MOSFET geometry, it was shown numerically that subband population plays a crucial role. In fact that investigation clearly showed that the behavior of α at the Fermi level is actually dictated by the competition of two processes: (i) an increase due to electric field and (ii) a decrease due to subband population.

In addition, despite obvious differences in device geometry, e.g., quantum well vs MOSFET, and the active material, e.g., InAs vs InGaAs, analogous behaviors for α were found for different systems.[5,12] In addition to the appealing physical aspects of the MOSFET, one also expects, on physical grounds, that the insight gained from its study can be used in the investigation of gated asymmetric quantum wells. This fact motivated us into extending our most recent work on this subject by focusing on another aspect not treated as yet in the existing literature, namely, the impact of the doping concentration on the electronic structure with special emphasis put on the zero-field spin splitting and particularly on the N_S dependence of α.

The paper is organized as follows: In Sec. II we discuss the electronic structure and its dependence on doping. Then in Secs. III and IV we present, respectively, the dependence of the spin splitting and Rashba parameter on the two-dimensional (2D) electron density N_S. In Sec. V we exhibit numerical simulations of SdH spectra and provide an analysis of the magnetoresistance measurements of Ref. 13, and finally in Sec. VI we conclude the paper and summarize the salient findings of this work.

II. ELECTRONIC STRUCTURE

We computed self-consistently the electronic structure of electrons bound within the inversion layer on *p*-InAs in a MOSFET geometry using our previous model.[5] In our present computations, the variables are the 2D electron density N_S and the volume density of ionized impurities N_A-N_D which we sweep, respectively, in the intervals $\sim 10^{11}-4.8\times10^{12}$ cm^{-2} and $1.8\times10^{15}-1.8\times10^{17}$ cm^{-3} with the material parameters being those of Ref. 5. We denote the dispersion of each one the energy spin-split branches by $\varepsilon_\nu^\sigma(k)$, where $\nu=0,1,...$, and $\sigma=\pm$ stand for the subband and spin indices, respectively, while k is the in-plane wave vector. Note that since the bulk contribution to spin splitting is small[21] for narrow gap semiconductors such as InAs, we limit ourselves only to the Rashba contribution. At $T=0$ K, the system is characterized by a Fermi energy E_F which depends both on N_S and N_A-N_D. For a given subband ν, the relation $\varepsilon_\nu^\sigma(k_F^{\nu\sigma})=E_F$ defines the fermi wave vectors $k_F^{\nu\pm}$ from which the subband occupations $N_{\nu\sigma}$ are straightforwardly computed. In addition, it is also useful for our discussion to define the intersubband splitting at $k=0$ between subband ν and ν' as $E_{\nu\nu'}=\varepsilon_{\nu'}(0)-\varepsilon_\nu(0)$; note that we do not specify σ because the two spin states are degenerate at the Brillouin zone center.

Figure 1 shows the Fermi energy E_F as a function of N_S for different values of the doping concentration N_A-N_D in the range 1.8×10^{15} cm$^{-3}-1.8\times10^{17}$ cm^{-3}. The 2D electron densities at which the first ($\nu=1$) and second ($\nu=2$) excited subbands start to populate are also marked, by circles (○) and triangles (△), respectively. As expected, e.g., from a triangular potential approximation,[22] one notes that E_F is an increasing function of both N_S and N_A-N_D; moreover, as higher subbands start to populate the slope dE_F/dNs diminishes somewhat and is always discontinuous at the onset of population of a new subband. In Fig. 2 we plot the intersubband energy $E_{\nu\nu'}$ vs N_S for different values of the doping concentration N_A-N_D. Note that the graphs are restricted only to N_S values where both subbands, i.e., ν and ν', are populated. For N_A-$N_D \geqslant 4.33\times10^{16}$ cm^{-3}, only two subbands are occupied because the high electric fields resulting from the high-doping concentrations produce large intersubband spacings which prevent higher subbands from being populated. One should also notice that $E_{01}>E_{12}$ for all values of N_S, in addition both E_{01} and E_{12} are increasing functions of both N_A-N_D and N_S; note also that the dependence

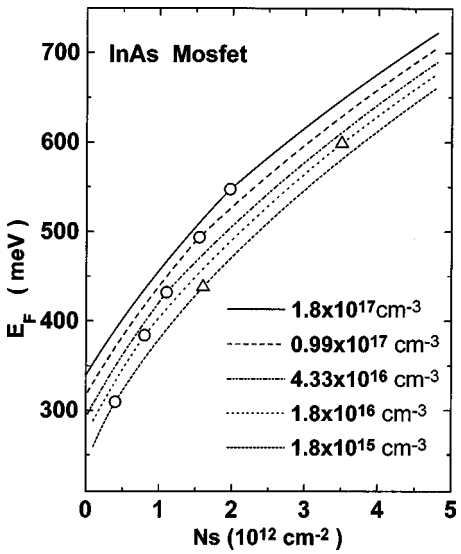

FIG. 1. Fermi energy as a function of the two-dimensional electron density N_S. The different curves are for various doping concentrations shown in the legend. Circles and triangles mark, respectively, the points where the first and second excited subbands start to be populated.

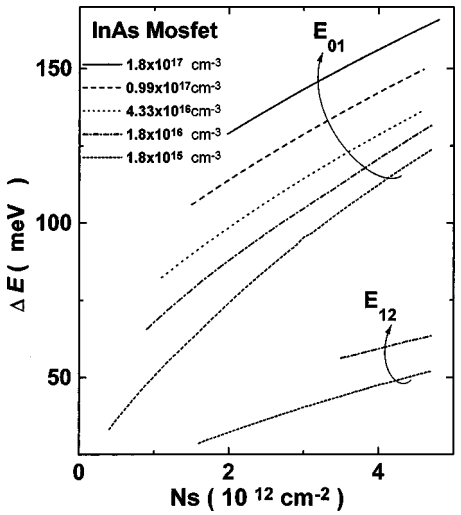

FIG. 2. Intersubband spacing $E_{\nu\nu'}=\varepsilon_{\nu'}(0)-\varepsilon_\nu(0)$ between subbands ν' and ν at the zone center as a function of the two-dimensional electron density N_S. The different curves are for various doping concentrations. E_{01} is between the ground and first excited subbands, while E_{12} is between the first and second excited ones.

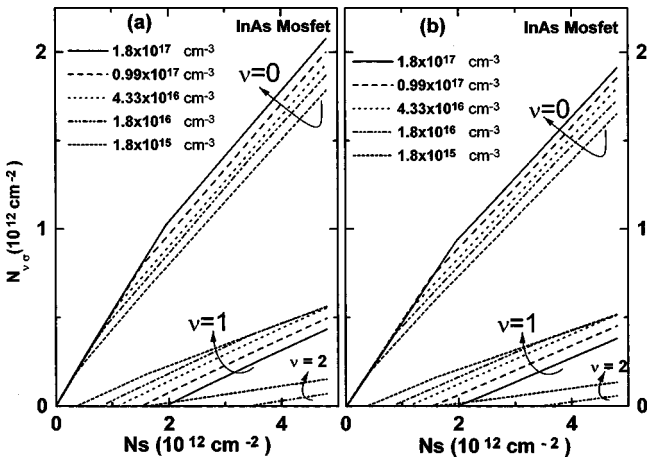

FIG. 3. Spin-split subband occupation $N_{\nu\sigma}$ as a function of the electron density N_S in the inversion layer, the various curves within each figure are for the different doping concentrations shown in the legend, and ν indicates the subband index. (a) and (b) are for the spin ''up'' and ''down'' branches, respectively.

on the latter is almost linear, and with this being slightly more so at higher values of N_A-N_D.

Figures 3(a) and 3(b) exhibit the occupancies of the spin-split subbands for $\nu=0\cdots2$ as functions of N_S at different values of N_A-N_D; note that both figures are drawn on the same scale to allow for comparison. For a given doping concentration, one notes that for all N_S the occupation numbers $N_{\nu+}$ and $N_{\nu-}$ are different from each other, although by small amounts. In experiments[8–14] this small difference usually leads to beatings in the SdH traces, although some exceptions to this rule have been pointed out.[15,16] The dependence of $N_{\nu\sigma}$ on N_S in Fig. 3 is nearly piecewise linear, nevertheless the slopes $dN_{\nu\sigma}/dNs$ before and after a new subband is occupied are different. For a fixed N_S, the occupation number $N_{0\sigma}$ in the ground subband increases as N_A-N_D increases contrary to the corresponding occupation number $N_{\nu\sigma}$ in higher subbands which is actually a decreasing function of N_A-N_D. This property is easily understood if we recall that as the doping concentration increases the intersubband spacing rises (see Fig. 2) thus making the ground and excited subbands accommodate more and fewer electrons, respectively.

III. ZERO FIELD SPIN SPLITTING

For $k>0$, in subband ν the zero-field spin splitting at wave vector k is $\delta_k^\nu=\varepsilon_\nu^-(k)-\varepsilon_\nu^+(k)$. This choice assures a positive δ_k^ν. In our work, our calculations show that for a fixed k, δ_k^0, and δ_k^1 increase almost linearly with N_S. Moreover, at a fixed electron density N_S, and for the same wave vector k, the spin splitting δ_k^0 in the ground subband is always larger than its counterpart δ_k^1 in the first excited subband. Furthermore, within the same subband and for a given N_S, the spin splitting δ_k^ν is usually an increasing function[23] of k.

The spin splitting at the Fermi level is given by $\delta_\pm^\nu=\delta_{kf}^\nu$, where kf stands for the Fermi wave vectors $k_F^{\nu\pm}$ already defined. Since the difference $\delta_+^\nu-\delta_-^\nu$ is usually small, and is not expected to have any experimental relevance, we instead use the average spin splitting at the Fermi level for subband ν, given by $\delta_\nu=\frac{1}{2}(\delta_+^\nu+\delta_-^\nu)$. Figure 4 shows δ_ν as a function of N_S for different doping concentrations in the range 0.433×10^{17}–1.8×10^{17} cm^{-3} where one first notes that $\delta_0>\delta_1$ for all N_S. Moreover, both δ_0 and δ_1 are increasing functions of electron density; note, however, that this dependence is not a linear one. In the ground subband, in addition to its increase with N_S, δ_0 is also an increasing function of the doping concentration N_A-N_D. This can easily be understood if we remember that as N_A-N_D gets larger, the electric field gets stronger and the Fermi wave vectors also get larger because of the larger intersubband spacing which pushes the population of the first excited subband to higher N_S. Both effects thus combine constructively to yield a larger spin splitting at the Fermi level. For the first excited subband, the dependence on N_A-N_D is slightly more complicated. In this regard, one should start first noting that the density N_S^1 at which the first excited subband populates depends quite sensitively on the doping concentration and varies roughly from 1.1×10^{12} cm^{-2} to 1.97×10^{12} cm^{-2} as N_A-N_D increases from 0.433×10^{17} cm^{-3} to 1.8×10^{17} cm^{-3}. This means that in higher subbands the Fermi wave vectors at which the spin splitting is computed (or measured) are smaller the larger the doping concentration is. Now one should not overlook that in contrast to $k_F^{1\pm}$ for $\nu=1$, the average electric field for electrons in the first excited subband in fact increases with N_A-N_D and since the spin splitting roughly increases, albeit in a complicated fashion,

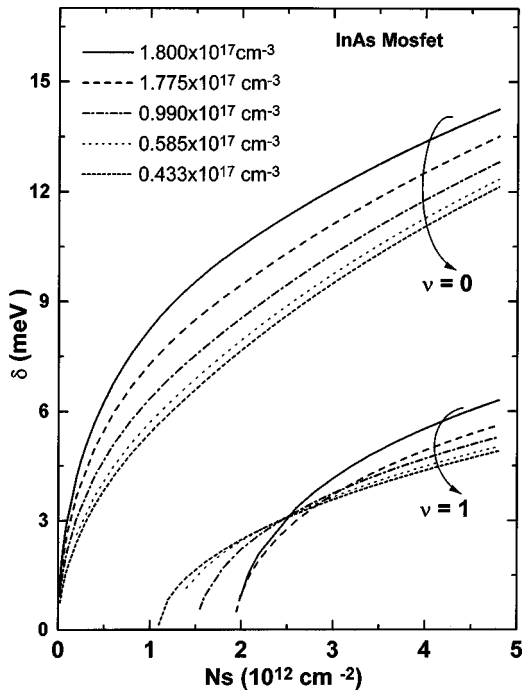

FIG. 4. Spin splittings δ_0 and δ_1 at the Fermi level in the ground and first excited subbands, respectively, as functions of the 2D electron density N_S at different doping concentrations. The greek letter ν stands for the subband index, with $\nu=0$ (1) for the ground (first excited) subband.

with both k and electric field it turns out that the outcome is not that obvious to predict for N_S close to N_S^1 but as we get away from the region $N_S \sim N_S^1$, both the electric field and Fermi wave vectors in the first excited subband increase enough to overcome the decrease in spin splitting that resulted from the smaller Fermi wave vectors near N_S^1. This explains why at higher N_S the behavior of δ_1 vs N_S as a function of N_A-N_D becomes similar to that of δ_0 in the ground subband discussed above.

IV. RASHBA PARAMETER

The Rashba model[18] for spin splitting describes spin-orbit effects in quasi-2D systems using an effective Hamiltonian H_{SO} given by

$$H_{\mathrm{SO}} = \alpha(\mathbf{k}\times\hat{x})\cdot\boldsymbol{\sigma}, \tag{1}$$

where $\mathbf{k}$, $\hat{x}$, and $\boldsymbol{\sigma}$ have their usual meaning.[5] The Rashba spin-orbit parameter α measures the strength of the spin-orbit interaction due to the electric field present within the inversion layer. As such, in Eq. (1) α depends on N_S and N_A-N_D only through the electric field. It was, however, shown that α was not dependent simply on the electric field but also depends on wave vector k. This k dependence could be either explicit or implicit through the energy and wave functions of the eigenstate under investigation. Therefore, we generalize Eq. (1) by letting α acquire a k dependence and define the new parameter α_k^ν by

$$\alpha_k^\nu = \frac{\delta_k^\nu}{2k}. \tag{2}$$

With this prescription, α_k^ν is positive and depends both on k and subband index ν. In Fig. 5 we plot this ν- and k-dependent Rashba parameter as a function of N_S for a doping concentration N_A-$N_D = 1.775\times10^{17}$ cm^{-3}. From this illustration one very clearly sees the following: (i) For a given k, the dependence of α_k^ν on N_S is almost linear. (ii) For a given k, we have $\alpha_k^0 > \alpha_k^1$ for all N_S; note, however, that this is no longer true if we compare the same parameters at different values of k even if N_S is the same. (iii) At a given electron density N_S, both α_k^0 and α_k^1 decrease as k increases.

As in Sec. III we also define the subband Rashba parameter at the Fermi level by

$$\alpha_\nu^\sigma = \frac{\varepsilon_\nu^-(k_F^{\nu\sigma}) - \varepsilon_\nu^+(k_F^{\nu\sigma})}{2k_F^{\nu\sigma}} \tag{3}$$

and introduce the average $\alpha_\nu = (\alpha_\nu^+ + \alpha_\nu^-)/2$ which depends only on ν. With N_A-N_D as a parameter, the dependence of α_ν on N_S in both the ground and first excited subbands are depicted, respectively, in Figs. 6 and 7 both of which show that the Rashba parameter is not N_S linear, nor is it even nearly so. One should also note that in Fig. 6 the Rashba parameter α_0 at the Fermi level shows a variety of new and intuitively unexpected behaviors as N_S is swept across. For instance, one easily distinguishes four different dependencies on N_S which in our case occur for the following doping concentrations: 1.8×10^{17} cm^{-3}, 1.775×10^{17} cm^{-3}, 0.99×10^{17} cm^{-3}, and 0.433×10^{17} cm^{-3}, respectively. The first one was already discussed in Ref. 5 and included here only for completeness. On the other hand, for the second case α_0

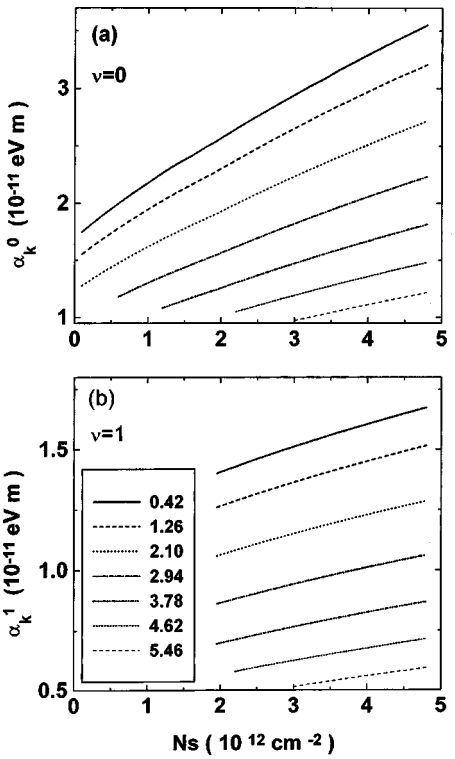

FIG. 5. The subband Rashba parameter at wave vector k as a function of electron density N_S. (a) and (b) are for the ground and first excited subbands, respectively, and the doping concentration N_A-N_D is 1.775×10^{17} cm^{-3}. The legend in (b) gives the values of the wave vector k in units of 10^8 m^{-1}, and is the same for (a).

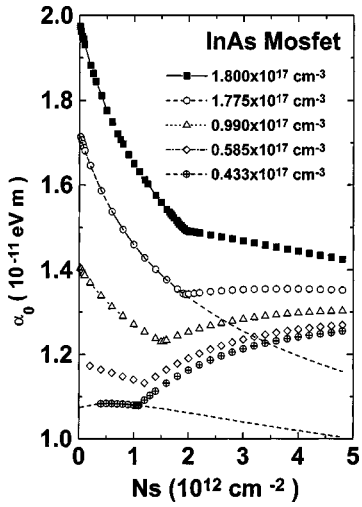

FIG. 6. The Rashba parameter α_0 at the Fermi level for electrons in the ground subband as a function of electron density N_S. The various curves are for different values of the doping concentration as shown in the legend. The dashed curves for N_A-$N_D = 0.433\times10^{17}$ cm^{-3} and N_A-$N_D = 1.775\times10^{17}$ cm^{-3} correspond to a fake situation where only one subband is occupied for all N_S.

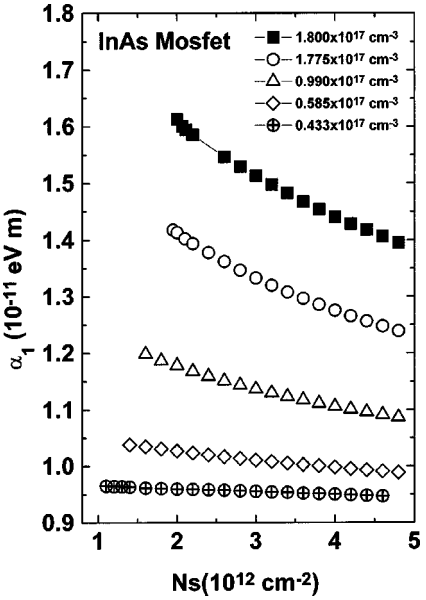

FIG. 7. Same as Fig. 6 but for electrons in the first excited subband.

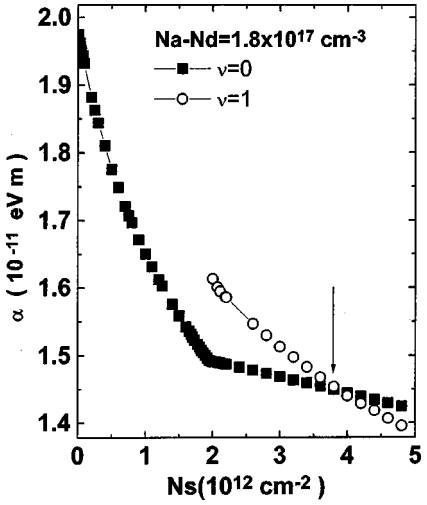

FIG. 8. Comparison between the Rashba parameter α_0 in the ground subband (filled squares) and α_1 in the first excited one (open circles) for a doping concentration of 1.8×10^{17} cm^{-3}, as a function of the 2D electron density N_S. The arrow points to where the two curves cross each other at $N_S=3.93\times10^{12}$ cm^{-2}.

first decreases as previously but starting at $N_S^1\cong1.95\times10^{12}$ cm^{-2} the curve levels off and α_0 becomes constant to better than 0.9% in a rather wide interval of the 2D electron density. This reminds one of the surprising result of Heida *et al.*[11] already mentioned. For the third case, α_0 first decreases up to $N_S\cong1.55\times10^{12}$ cm^{-2} then starts increasing again. Finally for the fourth case α_0 keeps a nearly constant value of 1.08×10^{-11} eV m up to $N_S\cong1.1\times10^{12}$ cm^{-2}, where it then starts increasing. In passing, note also that for a given N_S, α_0 increases with N_A-N_D, moreover for a given doping concentration the point where the curve α_0 vs N_S changes its trend with a concomitant discontinuity in the derivative $d\alpha_0/dN_S$ always coincides with the onset of filling in the first excited subband. These results are consistent with the experimental data of Hu *et al.*[12] on quantum wells already alluded to in Sec. I.

Figure 7 shows the N_S dependence of α_1 in the first excited subband, which is found to be a decreasing function of electron density for the values of N_A-N_D shown in the legend. For a doping concentration of 0.433×10^{17} cm^{-3} an almost constant value is found as compared to higher concentrations. We should also mention that, as for α_0, for a fixed N_S α_1 also increases with N_A-N_D.

Next, to resolve the question of how the Rashba parameter in the ground and first excited subbands compare to one another, for clarity we plot in Fig. 8 separately for N_A-$N_D=1.8\times10^{17}$ cm^{-3}, and on the same frame both α_0 and α_1 to allow for easy comparison. We very clearly see from that plot the existence of a density $\tilde{N}_S^0\cong3.93\times10^{12}$ cm^{-2} for which $\alpha_0=\alpha_1$. Moreover, for $N_S>\tilde{N}_S^0$ we have $\alpha_0>\alpha_1$ whereas for $N_S<\tilde{N}_S^0$ we have $\alpha_0<\alpha_1$ instead. To the best of our knowledge this crossing is predicted here for the first time. In addition note that for N_A-$N_D=1.775\times10^{17}$ cm^{-3} a basically analogous behavior is found, the only difference being the electron density $\tilde{N}_S^0$ where the crossing occurs, which in this case is roughly equal to 2.75×10^{12} cm^{-2}. For the other values of the doping concentration we always have $\alpha_0>\alpha_1$ regardless of N_S.

To understand the behavior of the Rashba parameter as a function of N_S, we consider the mechanisms which have a direct link with α_ν. To this end, for N_A-$N_D=1.775\times10^{17}$ cm^{-3} we plot in Fig. 9 the ν- and k-dependent Rashba parameter α_k^ν as a function of k at different values of

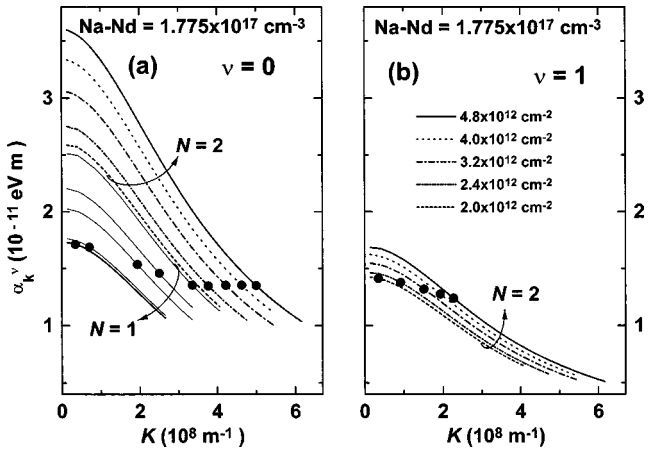

FIG. 9. Line graphs: Subband Rashba parameter α_k^ν as a function of wave vector k at different values of the 2D electron density N_S. Filled circles: Rashba parameter at the Fermi level as a function of the average Fermi wave vector; the frames (a) and (b) are, respectively, for the ground ($\nu=0$) and first excited ($\nu=1$) subbands, and in each case N denotes the number of occupied subbands for the relevant group of curves. The doping concentration is N_A-$N_D=1.775\times10^{17}$ cm^{-3}. The legend in (b) gives the electron density N_S for each curve, and is the same for the corresponding curves in (a). Moreover, in panel (a), the lower embraced curves labeled with $N=1$ correspond to low electron densities N_S where only one subband is occupied.

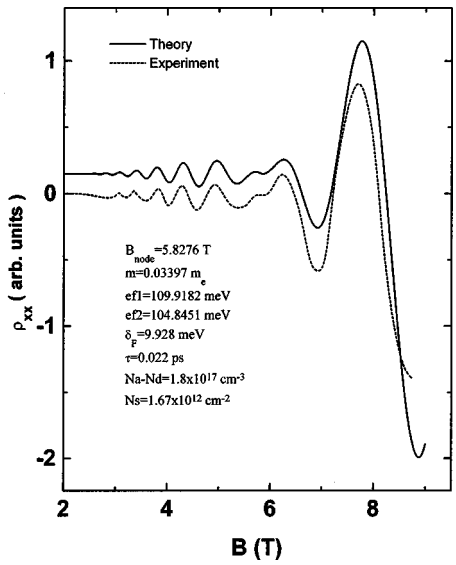

FIG. 10. Comparison between the experimental SdH trace of Ref. 13 and our own theoretical simulation in the present work. In the legend $B_{\rm node}$ stands for B_0 the value of the magnetic field where the node of the beating pattern occurs while ef1 and ef2 are our best fit values for the Fermi energy, as measured from the bottom of the subband, for magnetic fields B smaller and larger than B_0, respectively.

N_S. Moreover, to examine the relationship that exists between α_0 and α_1 and how it arises, plots for $\nu=0$ and $\nu=1$ are drawn on the same scale. In Figs. 10(a) and 10(b) the k-dependent Rashba parameters α_k^0 and α_k^1 are plotted as line graphs, while α_0 and α_1 are represented by symbols. One obviously notices that in both subbands α_k^ν is maximal at $k=0$ but as k increases this parameter decreases very strongly. Furthermore, at a fixed wave vector k, α_k^ν increases with N_S, and if we compare α_k^ν in the ground and first excited subband we clearly see that for the same k and N_S this parameter is higher in the ground subband. Note, however, that if we compare these parameters for the same N_S but at different k values in both subbands, this is no longer true and depending on the values of these wave vectors we may have all three possible cases. The data shown in figs. 10(a) in particular the N_S dependence of α_0, deserve a few comments. Indeed we see that as we increase N_S two aspects appear: (i) the whole curve representing α_k^0 shifts upward (this simply means that α_k^0 increases for all k) and (ii) the Fermi wave vector at which α_0 is computed increases, i.e., the symbols representing the data points shift to the right. While process (i) tends to increase α_0, process (ii), on the other hand, tends to decrease it. The overall trend of α_0 as a function of N_S therefore depends on the delicate balance of these two processes. When process (i) is dominant we have an increasing trend, on the contrary if process (ii) is dominant we will have a decreasing trend, finally if both are equal they cancel each other and a constant value for α_0 obtains. For N_A-$N_D=1.775\times10^{17}$ cm^{-3} comparison between Figs. 9(a) and 9(b) shows that although we always have $\alpha_k^0>\alpha_k^1$ for the same N_S, at the Fermi level we may have $\alpha_0\leqslant\alpha_1$ for $N_S\leqslant2.75\times10^{12}$ cm^{-2} because the Fermi wave vectors in the first excited subband are smaller than their homologues in the ground subband. This argument is also behind the crossing shown on Fig. 8 for N_A-$N_D=1.8\times10^{17}$ cm^{-3}.

Finally, for N_A-$N_D=1.775\times10^{17}$ cm^{-3} and 0.433×10^{17} cm^{-3} we show on Fig. 6 as dashed curves the influence of the first excited subband on α_0. For this purpose, in addition to our calculations already discussed in the text, in both cases we also compute the electronic structure assuming a fake situation where for all N_S only one subband is occupied, α_0 is then deduced under this constraint. One can easily notice that in this artificial scenario, α_0 is simply a decreasing and smooth function of density N_S with no discontinuities in its derivative with respect to N_S anywhere. Note also that for the same electron density N_S, because occupation of the first excited subband in the real situation reduces the Fermi wave vectors in the ground subband (because the first excited subband competes with it), this fact alone yields larger values for α_0 than if the ground subband were the only one occupied. As a consequence, for N_A-$N_D=1.775\times10^{17}$ cm^{-3} α_0 stops decreasing and becomes nearly constant for $N_S\geqslant1.95\times10^{12}$ cm^{-2}, on the other hand for N_A-$N_D=0.433\times10^{17}$ cm^{-3} occupation of the first excited subband leads to an increasing trend for α_0 for $N_S\geqslant1.1\times10^{12}$ cm^{-2}.

V. SIMULATION AND ANALYSIS OF EXPERIMENTAL SdH SPECTRA

To bridge the gap between experiment and our present theoretical work, in this section we simulate the SdH spectra using the very recent theory of Tarasenko and Averkiev[25] which has the merit of simplicity. In addition within the premises of the model adopted by these authors we also analyze the experimental data of Ref. 13 where we should recall that only one beating node was observed. Furthermore, as compared to other similar experiments,[8–12,14,16,17] in Ref. 13 the magnetic field strengths at which this unique node was seen are rather moderate despite the smaller effective mass of InAs. This could hint to the lower quality for transport which may be inherent to the MOSFET geometry. This may be due to interface imperfections, for instance, as well as impurity scattering because of the high doping concentration and the random bulk distribution of dopants in the sample as opposed to the much better interface quality and modulation doping in quantum wells.

The theory of Ref. 25 gives the position of the lth order node as

$$B_l=\frac{2\,\delta m^*}{(2l+1)e\hbar}, \tag{4}$$

where δ and m^* are the zero-field spin splitting and effective mass at the Fermi level while $l=0,1,...,$ is a non-negative integer. In our analysis we use our theoretical values of Sec. III for δ. In addition we read the node position graphically from the reported experimental traces.[13] Next using Eq. (4) we infer m^* which we compare with the experimental cy-

clotron mass and our own zero-field density of state (DOS) mass. Furthermore we deduce the values of the Fermi energy using the relation

$$E_F' = \frac{\hbar e}{m^* T_B}, \tag{5}$$

where T_B is the period of SdH oscillations when plotted as a function of $1/B$ while E_F' is the Fermi energy in the presence of the magnetic field measured from the bottom of the subband.[25] After the appropriate modifications related to the origin of the energy scale are made, the values obtained for E_F' are compared to our zero-field Fermi energies discussed in Sec. II. Finally the number of observed nodes as well as the heights of the various maxima are used to choose the adequate scattering time τ. In this regard, it should be mentioned that τ is a measure of the Dingle temperature T_D and is different from the transport relaxation time;[26] moreover, it basically has no influence on the position of the node or the period of oscillations.

For our fit we choose to reproduce the uppermost curve corresponding to $V_g = 30$ V in Fig. 1 of Ref. 13 because its node is more easily identified compared to lower gate voltages. Its fast Fourier transform shown on panel (b) of the same figure yields straightforwardly the occupation numbers $N_\pm$ which are found to be 0.935×10^{12} and 0.74×10^{12} cm^{-2} while our zero-field theory predicts 0.8800×10^{12} and 0.794×10^{12} cm^{-2}, respectively, i.e., an accuracy better than $\sim 6\%$. Considering the high magnetic fields used in experiment and the limitations[27] of the SdH method to predict $N_\pm$ we consider the agreement to be very good. The contributions N_+ and N_- of the two branches add up to $N_S = 1.674 \times 10^{12}$ cm^{-2} in excellent agreement with the value 1.602×10^{12} cm^{-2} obtained from the experimental SdH oscillations' period.

In Fig. 10 we compare the experimental SdH oscillations of Matsuyama *et al.*[13] with our own simulation using for the conductivity tensor Eqs. (5) and (6) of Ref. 25. Note that in Fig. 10 our theoretical curve is slightly shifted upward on purpose for clarity. Note also that only the 0th node is resolved and is located at $B_0 = 5.828$ T. Using the theoretical value $\delta = 9.93$ meV, the value of B_0 above, and Eq. (4) with $l = 0$ yield $m^* = 0.034\, m_e$. For comparison for the same electron density, our zero field DOS mass is $0.042 m_e$ while estimation[13] of the experimental cyclotron mass would give $0.029 m_e$. It is clear that the value of m^* obtained in our best fit is smaller than the theoretical DOS mass and larger than the cyclotron mass. This can easily be understood if we recall that the B field lowers the Fermi energy due to the large degeneracy of the Landau levels. Since the mass is energy dependent due to nonparabolicity one expects a smaller mass[28] than in the $B = 0$ case, which is confirmed here. To explain the slightly smaller cyclotron mass, we should have in mind that SdH oscillations are magnetotransport properties and as such should only involve levels around the Fermi energy whereas the cyclotron resonance process couples Landau levels that differ from each other by a finite quantum that is equal to the laser photon energy $h\nu$. Unfortunately, the resonant magnetic field and the photon energy used in the CR experiment were not given by the authors in Ref. 13, and we know that nonparabolicity makes the cyclotron mass magnetic field, Landau index, and electron density dependent, strict quantitative comparison here is therefore not possible. We should, however, point out that our results are consistent with older SdH and CR experiments on electrons in the inversion layer of the Si MOSFET where SdH masses are found to be slightly larger than CR masses.[29] Furthermore, it would be desirable if the temperature dependence of the SdH spectrum be investigated experimentally by the authors of Ref. 13 in order to deduce the effective mass of the electrons at the Fermi level and see how it would compare to their own cyclotron mass. Next, using m^* from our fit we further find $E_F' = 109.92$ meV for $B < B_0$ and 103.26 meV for $B > B_0$ in contrast to $E_F' = 113.22$ meV obtained from our zero-field theory. The agreement is therefore excellent, and we should emphasize that these values are consistent with the argument given above regarding the lowering of the Fermi energy. Subsequently, using $\tau \cong 2.2 \times 10^{-14}$ s we reproduce very properly all the features displayed by the experimental SdH trace. The rather small value of τ can be attributed to the increase of scattering chances due to (i) the high doping concentration of ionized impurities and (ii) interface roughness whose effect is expected to be felt more strongly when doping is higher because the electrons are more tightly bound to the interface and therefore feel the latter much more. Moreover, we should stress in this regard that scattering by acoustic phonons also should not be overlooked since the experiment of Ref. 13 was carried at $T = 2$ K as opposed to 0.4 K in Refs. 9 and 12, 0.3 K in Ref. 8, and 0.05 K in Ref. 10.

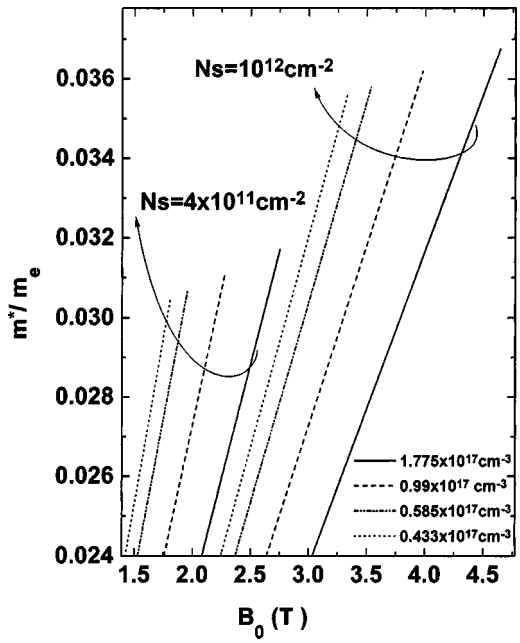

FIG. 11. Effective mass m^* (as would be measured by an SdH experiment) as a function of the zeroth order node magnetic field B_0 for two 2D electron densities N_S and several doping concentrations N_A-N_D.

Using the theoretical values of the spin-splitting δ as predicted here, we display in Fig. 11 the position of the 0th node as a function of the effective mass m^* taken as an unknown

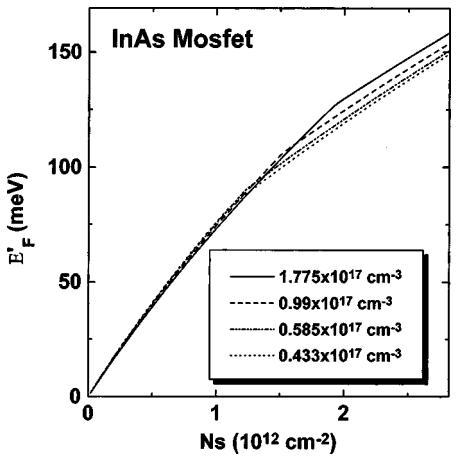

FIG. 12. Fermi energy E_F' (measured from the bottom of the ground subband), for several doping concentrations N_A-N_D, as a function of the 2D electron density N_S.

parameter to be determined by further experimental work. Moreover Eq. (5) above coupled with Fig. 11 should allow for the determination of E_F' which must have as an upper bound our zero-field value of the same parameter which we plot separately in Fig. 12 for completeness. The only remaining parameter τ depends on the quality of the sample and can be deduced phenomenologically by trial and error using the experimental SdH traces to be reproduced.

VI. CONCLUSIONS

To summarize, using the envelope function scheme and the 8×8 Kane $\mathbf{k}\cdot\mathbf{p}$ Hamiltonian[24] we studied theoretically within the self-consistent Hartree approximation the influence of the doping concentration on the electronic structure and particularly on the zero-field spin splitting and corresponding Rashba parameter of electrons bound within the inversion layer on *p*-InAs in a MOSFET. We computed many physical quantities of interest such as the spin split subband occupancies, the spin splitting at the Fermi level, the Rashba spin-orbit parameter, and investigated in detail the dependence of these on the 2D electron density and doping concentration.

By varying the doping concentration in the range 0.433×10^{17}–1.8×10^{17} cm^{-3}, at the Fermi level, for the Rashba parameter we discover new N_S dependencies. Moreover for InAs MOSFETs, we infer from our calculations that for N_A-$N_D>1.775\times10^{17}$ cm^{-3} the ground subband Rashba parameter α_0 should be a decreasing function of N_S, whereas for N_A-$N_D<0.433\times10^{17}$ cm^{-3} it should be increasing with N_S instead.

Furthermore, although the spin splitting in the ground subband is always larger than in the first excited subband, which is also true for the Rashba parameter at a given wave vector k, at the Fermi level we show that at high doping concentrations and for N_S in a given interval the Rashba parameter in the first excited subband actually exceeds its counterpart in the ground subband because the latter is evaluated at much larger Fermi wave vectors. As N_S is increased, both become equal and then this coefficient becomes larger in the ground subband. For low-doping concentrations however, we always have smaller Rashba parameters in higher subbands. These behaviors are naturally explained in the text as arising from the strong k dependence of α_k^ν.

We expect the dependencies found in our work to also be present in asymmetric/symmetric gated and/or doped quantum wells and could in principle be observable for wide wells where the low-lying eigenstates are expected to behave as in our case. In Ref. 3 the authors find that the dependence of the spin splitting δ_k^ν on subband index ν is tied to the shape of the confining potential. However, only two types of potential wells were considered there. For instance, these authors did not consider a square well with a gate which when the well is wide and the electric field is strong enough would on physical grounds be expected to behave as a heterojunction because the probability for an electron to reach the interface farthest from the gate is negligible. Furthermore, in Ref. 12 the authors suggest that the Rashba parameter in the first excited subband could be larger or smaller than that in the ground subband. This statement is, however, true only for the Rashba parameter measured by transport experiments at the Fermi level. In addition, our present work stresses the importance of the k dependence of α_k^ν which turns out to be of paramount importance. In our opinion, at present we believe that more theoretical work is still needed to assess more quantitatively the relative roles of the confining potential, tunneling into the barriers, and nonparabolicity in order to reach a unified picture.

Furthermore, we hope that the present theoretical study will stimulate more experimental investigations both on MOSFET's and wider quantum wells as suggested above using SdH techniques as well as other alternative means such as Raman scattering,[7] electron-spin resonance,[30] far-infrared magneto-optical absorption,[31] and interband tunneling spectroscopy[32] to gain a thorough understanding of this exciting subject.

ACKNOWLEDGMENTS

The author is very much indebted to Professor U. Rössler and his group, as well as to Dr. R. Winkler for the kind hospitality extended to him at Universität Regensburg and Universität Erlangen-Nürnberg, respectively. He is very thankful to both institutions for generously making their facilities available to him, and also thanks the Algerian ministry of higher education for a research grant.

*Email address: s_lamari@yahoo.fr

[1] S. Datta and B. Das, Appl. Phys. Lett. **56**, 665 (1990).
[2] P. Pfeffer and W. Zawadzki, Phys. Rev. B **52**, R14 332 (1995).
[3] E. A. de Andrada e Silva, G. C. La Rocca, and F. Bassani, Phys. Rev. B **55**, 16 293 (1997).
[4] P. Pfeffer, Phys. Rev. B **55**, R7359 (1997).
[5] S. Lamari, Phys. Rev. B **64**, 245340 (2001); J. Appl. Phys. **91**, 1698 (2002).

[6] R. Winkler, H. Noh, E. Tutuc, and M. Shayegan, cond-mat/0106246 (unpublished).
[7] B. Jusserand, D. Richards, G. Allan, C. Priester, and B. Etienne, Phys. Rev. B **51**, 4707 (1995).
[8] G. Engels, J. Lange, Th. Schäpers, and H. Lüth, Phys. Rev. B **55**, R1958 (1997).
[9] J. Nitta, T. Akazaki, H. Takayanagi, and T. Enoki, Phys. Rev. Lett. **78**, 1335 (1997); Physica E **2**, 527 (1998).
[10] Th. Schäpers, G. Engels, J. Lange, Th. Klocke, M. Hollfelder, and H. Lüth, J. Appl. Phys. **83**, 4324 (1998).
[11] J. P. Heida, B. J. van Wees, J. J. Kuipers, T. M. Klapwijk, and G. Borghs, Phys. Rev. B **57**, 11 911 (1998).
[12] Can-Ming Hu, J. Nitta, T. Akazaki, H. Takayanagi, J. Osaka, P. Pfeffer, and W. Zawadzki, Phys. Rev. B **60**, 7736 (1999); Physica E **6**, 767 (2000).
[13] T. Matsuyama, R. Kürsten, C. Meißner, and U. Merkt, Phys. Rev. B **61**, 15 588 (2000).
[14] D. Grundler, Phys. Rev. Lett. **84**, 6074 (2000).
[15] S. Brosig, K. Ensslin, R. J. Warburton, C. Nguyen, B. Brar, M. Thomas, and H. Kræmer, Phys. Rev. B **60**, 13 989 (1999).
[16] A. C. H. Rowe, J. Nehls, R. A. Stradling, and R. S. Ferguson, Phys. Rev. B **63**, 201307 (2001).
[17] Y. Sato, T. Kita, S. Gozu, and S. Yamada, J. Appl. Phys. **89**, 8017 (2001); Physica E **10**, 77 (2001).
[18] E. I. Rashba, Fiz. Tverd. Tela. **2**, 1224 (1960) [Sov. Phys. Solid State **2**, 1109 (1960).]; Y. A. Bychkov and E. I. Rashba, J. Phys. C **17**, 6039 (1984).
[19] J. Luo, H. Munekata, F. F. Fang, and P. J. Stiles, Phys. Rev. B **41**, 7885 (1990).
[20] We limit here our discussion to systems with only one gate as opposed to those with a backgate as well, where the electric field and the electron density can be monitored separately.
[21] G. Lommer, F. Malcher, and U. Rößler, Phys. Rev. Lett. **60**, 728 (1988).
[22] T. Ando, A. B. Fowler, and F. Stern, Rev. Mod. Phys. **54**, 466 (1982).
[23] For a given N_S, at large enough in-plane wave vectors k, the spin splitting actually saturates and then decreases slightly, see Ref. 5 for details.
[24] Evan O. Kane, J. Phys. Chem. Solids **1**, 249 (1957).
[25] S. A. Tarassenko and N. S. Averkiev, JETP Lett. **75**, 552 (2002).
[26] P. T. Coleridge, Semicond. Sci. Technol. **8**, 961 (1990).
[27] S. Keppeler and R. Winkler, Phys. Rev. Lett. **88**, 046401 (2002); R. Winkler, S. J. Papadakis, E. P. De Poortere, and M. Shayegan, *ibid.* **84**, 713 (2000).
[28] S. Lamari, Phys. Lett. A **200**, 387 (1995).
[29] T. Ando, A. B. Fowler, and F. Stern, Rev. Mod. Phys. **54**, 557 (1982) (see Fig. 134).
[30] Z. Wilamowski and W. Jantsch, Physica E **12**, 439 (2002).
[31] Ken-ichi Fujii *et al.*, Physica E **12**, 432 (2002).
[32] Kanji Yoh *et al.* (unpublished).